Thermodynamics of soluble fission products cesium and iodine in the Molten Salt Reactor

Capelli, E.; Beneš, O.; Konings, R. J.M.

DOI
10.1016/j.jnucmat.2018.01.024

Publication date
2018

Document Version
Final published version

Published in
Journal of Nuclear Materials

Journal of Nuclear Materials 501 (2018) 238–252

Contents lists available at ScienceDirect

Journal of Nuclear Materials

journal homepage: www.elsevier.com/locate/jnucmat

Thermodynamics of soluble fission products cesium and iodine in the Molten Salt Reactor

E. Capelli [a, b, *], O. Beneš [c], R.J.M. Konings [a, c]

[a] Department of Radiation Science and Technology, Faculty of Applied Sciences, Delft University of Technology, Delft 2629JB, The Netherlands
[b] Nuclear Research and Consultancy Group (NRG), 1755LE Petten, The Netherlands
[c] European Commission, Joint Research Centre, 76125 Karlsruhe, Germany

GRAPHICAL ABSTRACT

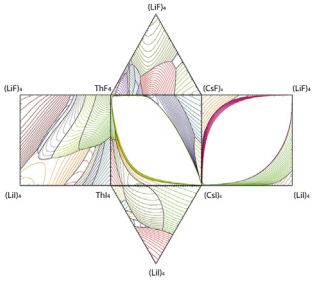

ARTICLE INFO

Article history:
Received 18 December 2017
Received in revised form
12 January 2018
Accepted 12 January 2018
Available online 6 February 2018

Keywords:
Molten Salt Reactor
Phase diagrams
Fission products
Cesium
Iodine
Fluoride salts

ABSTRACT

The present study describes the full thermodynamic assessment of the Li,Cs,Th//F,I system. The existing database for the relevant fluoride salts considered as fuel for the Molten Salt Reactor (MSR) has been extended with two key fission products, cesium and iodine. A complete evaluation of all the common-ion binary and ternary sub-systems of the LiF-ThF_4-CsF-LiI-ThI_4-CsI system has been performed and the optimized parameters are presented in this work. New equilibrium data have been measured using Differential Scanning Calorimetry and were used to assess the reciprocal ternary systems and confirm the extrapolated phase diagrams. The developed database significantly contributes to the understanding of the behaviour of cesium and iodine in the MSR, which strongly depends on their concentration and chemical form. Cesium bonded with fluorine is well retained in the fuel mixture while in the form of CsI the solubility of these elements is very limited. Finally, the influence of CsI and CsF on the physico-chemical properties of the fuel mixture was calculated as function of composition.

1. Introduction

The Molten Salt Reactor (MSR) is one of the promising reactor technologies considered for future nuclear energy development. Fissile and fertile materials are dissolved in a liquid molten salt mixture circulating in the primary circuit and serving both as fuel and as coolant for the fission reaction. Among the various design concepts, the focus in Europe is on the Molten Salt Fast Reactor (MSFR) [1,2] which exploits the advantages of a fast neutron spectrum. The reference salt for this concept is the binary LiF-ThF_4 eutectic mixture with addition of either UF_4 or PuF_3 [3] as fissile

* Corresponding author. Department of Radiation Science and Technology, Faculty of Applied Sciences, Delft University of Technology, Delft 2629JB, The Netherlands.
E-mail address: e.capelli@tudelft.nl (E. Capelli).

https://doi.org/10.1016/j.jnucmat.2018.01.024

and small concentration of UF_3 for the redox control.

In case of multi-component mixtures, the physico-chemical properties of the liquid salts can be effectively described by thermodynamic models and an extensive thermodynamic database including the most relevant systems for the MSR is being developed at the Joint Research Centre (JRC) since several years. However, at present the database considers mainly "fresh" fuel compositions, i.e. at the beginning of the reactor operation time. During irradiation, fission products are formed by the fission reaction and accumulate in the fuel matrix. The effect of this composition change on the melting behaviour, solubility limit and vapour pressure of the fuel must be carefully evaluated and could be achieved by extending the present thermodynamic database to the main fission products. The present work considers the effect of two of the most important fission products, cesium and iodine, on the fuel mixture. Both elements are produced with relatively high yield and deserve strong attention due to their volatility and radiological effects in accidental scenarios. Once formed, cesium and iodine are expected to dissolve in the $Li_xTh_{1-x}F_{4-3x}$ liquid solution and bond in the fuel.

In the present work, the modified quasi-chemical model in the quadruplet approximation was applied to describe the reciprocal Li,Cs,Th//F,I system. All the common-ion binary sub-systems have been reviewed and, if needed, newly assessed. Slight modifications have been made for the CsF- and CsI- containing phase diagrams due to a recent re-evaluation of their thermodynamic properties. The ternary common-ion systems (such as the LiF-CsF-ThF_4) and the reciprocal systems (Li,Cs//F,I; Cs,Th//F,I and Li,Th//F,I) were extrapolated and optimized in this work based on novel experimental data. The Differential Scanning Calorimetry (DSC) was used to determine the phase equilibria of the selected compositions and to confirm the extrapolated phase diagrams. Finally, the developed model was employed to investigate the behaviour of cesium and iodine in the specific case of the molten salt fuel mixture. The calculations aimed to evaluate the influence of CsF and CsI accumulation in the fuel on its critical thermodynamic properties, such as the melting temperature and the vapor pressure.

2. Experimental

2.1. Sample preparation

In order to complement the existing available data and confirm the developed thermodynamic model, selected compositions of the Li,Cs, Th//F,I system were synthesized and analysed in this work. The samples were prepared starting from the pure compounds lithium fluoride (LiF), cesium fluoride (CsF) and cesium iodide (CsI), obtained for Alfa Aesar, and thorium tetrafluoride (ThF_4), obtained from IBI Labs, USA. The details on the provenance of the samples, their purity and the treatments performed prior the mixing are summarized in Table 1. While LiF was provided in anhydrous form, CsF and CsI have been dried at 573 K for several hours under Ar flow to remove the residual moisture, if present. ThF_4 is likely to contain, in addition to moisture, oxide and oxyfluoride impurities which can be detected by calorimetric techniques and must be therefore removed from the samples. The purification process is described in details in Ref. [4] and is based on the conversion of oxides into fluorides using NH_4HF_2 as fluorinating agent. The purity of all the compounds has been confirmed using the DSC technique for the identification of the melting point. As reported in Table 1, the experimental values agree well with the literature values in all cases, within the instrument uncertainty (±5 K), confirming the purity of the samples.

The samples were prepared by mixing stoichiometric quantities of the end-members and were handled at any time under controlled atmosphere. An argon-filled glove box was used, in which the content of oxygen and water is constantly monitored and kept low, typically below 5 ppm. Moreover, in order to avoid the contact between the corrosive gas formed at high temperature and the environment of the instrument, the samples were encapsulated during the measurements. A gas tight stainless steel crucible internally lined with nickel is used as described in Ref. [8]. This method minimizes also the sample loss and the composition shift due to incongruent vaporization.

2.2. Differential Scanning Calorimetry

The Differential Scanning Calorimetry (DSC) is a widely used technique for the identification of phase equilibria in multi-component systems and was employed in this work to investigate the Li,Cs, Th//F,I system. The detector of the instrument, a Setaram MultiHTC-96 DSC suitable for temperature up to 1400 °C, is composed of two ceramic chambers, one for the sample and one for the reference, linked together by a series of interconnected S-types thermocouples. In this configuration, the heatflow between the two chambers is measured as function of temperature providing information on the occurence of temperature-induced process, such as phase transitions, visualized as peaks. The temperature of the transition and its energy can be determined from the analysis of the peak as the onset temperature and the area, respectively. For this purpose, a temperature calibration is required and was performed by measuring the melting point of several standard materials (In, Sn, Pb, Al, Ag, Au, Zn) with determined uncertainty of ±5 K. Argon was used as flowing inert purge gas for all measurements.

A standard measurement program was applied for all the samples and consists of four successive heating cycles with constant heating rate of 10 K/min, and different cooling rates (5 K/min, 7 K/min, 10 K/min and 15 K/min). During the first heating ramp, the samples were homogenized while the data were collected during the three following cycles. It is important to mention that CsI and CsF are quite volatile compared to the other components and partial vaporization might occur at high temperature leading to a composition shift. This process will have an effect mainly on the liquidus transition and can be identified by monitoring the variation of the temperature for the same transition in the subsequent cycles.

3. Thermodynamic modeling

3.1. Chemical forms of cesium and iodine

A preliminary thermochemical analysis was performed to identify the relevant species which have to be included in the

Table 1
Details on the provenance, the treatments and the purity of the compounds used in this work.

Compound	Provenance	Purity	Further treatment	$T_{melting}$/K	
				Exp.	Lit.
LiF	Alfa Aesar	99.99%	none (ultradry)	1118 ± 5	1121.3 ± 1 [5]
CsF	Alfa Aesar	99.99%	Drying (Ar atmosphere)	972.7 ± 5	976 ± 2 [5]
CsI	Alfa Aesar	99.999%	Drying (Ar atmosphere)	902.2 ± 5	905 ± 2 [6]
ThF_4	IBI Labs	99.99%	Purification using NH_4HF_2	1383.6 ± 5	1383 ± 3 [7]

Table 2
Possible stable chemical forms of cesium and iodine in fluorine-containing environment considered in this work.

Fission products	Chemical species
Cesium	CsI CsF Elemental gases (Cs, Cs_2)
Iodine	CsI LiI ThI_4 Elemental gases (I, I_2) IF_x (g)

database. A list of possible chemical forms of cesium and iodine in fluoride salts is given in Table 2. In normal operation conditions, our preliminary thermodynamic calculations predicts negligible presence of the elemental gases (I, I_2, Cs, Cs_2) as well as for the gaseous IF_x compounds, which are likely to be formed only at rather high fluorine potential. Iodine is indicated to be in the form of iodide and the description of the full system can be achieved considering cations (Li^+, Cs^+, Th^{4+}) and anions (F^-, I^-) in a reciprocal system, written as Li,Cs,Th//F,I.

The average exchange Gibbs energy for the pure liquid salts in the system were also calculated over the temperature range 600–1500 K and are given below.

$$LiI + CsF \rightarrow LiF + CsI \qquad \Delta g^{exchange} \simeq -106.5\ \text{kJ}$$
$$ThI_4 + CsF \rightarrow ThF_4 + CsI \qquad \Delta g^{exchange} \simeq -143.6\ \text{kJ}$$
$$LiF + ThI_4 \rightarrow LiI + ThF_4 \qquad \Delta g^{exchange} \simeq -37.1\ \text{kJ}$$

Based on these calculations, CsI is expected to be the most stable of the possible iodides in the liquid solution causing a strong short range order. Hence, particular emphasis was paid in the present work to the description of the CsI-containing sub-systems in addition to the fluorides. It must be noted here that only a minor part of the total cesium produced can form CsI as the iodine is produced with a much lower yield compared to cesium, the molar ratio Cs/I being about 10. At this stage, the thermochemical analysis does not take into account the interaction of cesium and iodine with the other fission products (such as the formation of $CsTe_x$) or the possible interaction with structural materials.

3.2. Compounds

The studied system contains five different ions: three cations (Li^+, Cs^+, Th^{4+}) and two anions (F^-, I^-). The two by two combinations generate six pure compounds LiF, CsF, ThF_4, LiI, CsI, ThI_4, which have to be described in the thermodynamic model. The thermodynamic stability of all the compounds is given by their Gibbs energy defined as:

$$G(T) = \Delta_f H^0(298) - S^0(298)T + \int_{298}^{T} C_p(T)\mathrm{d}T - T\int_{298}^{T}\left(\frac{C_p(T)}{T}\right)\mathrm{d}T, \qquad (1)$$

where $\Delta_f H^0(298)$ and $S^0(298)$ are respectively the standard enthalpy of formation and standard absolute entropy, both referring to a temperature of 298.15 K and $C_p(T)$ is the temperature function of the heat capacity at constant pressure. The thermodynamic data for all compounds used in this work are reported in Table 3 and have been taken from the literature works cited therein. The enthalpy of formation of two intermediate compounds, $LiCsF_2$ and Cs_2ThI_6, have been optimized in this work while their standard entropy and the heat capacity values were calculated as weighted average of the end-members properties (Neumann-Kopp rule in case of heat capacity). Finally, the thermodynamic properties of four intermediate compounds in the LiI-ThI_4 system were estimated as discussed in the next section.

Since CsI and CsF have a relatively high vapour pressure compared to the other salts and given the importance of the vaporization behaviour of fission products in the molten salt mixture, the gaseous species have also been included in the model. The thermodynamic properties of the gaseous phases used in this work are reported in Table 4 and have been taken from the literature works cited therein.

3.3. Liquid solution

The liquid solution was treated in this work using the modified quasi-chemical model proposed by Pelton et al. [14]. This model is very suitable to describe molten ionic solutions as the composition of maximum short range ordering (SRO) is permitted to vary by changing the defined "coordination numbers" $Z^i_{AB/XY}$. The species in solution are distributed over two sublattices, typically the cations A,B,C,…on one sublattice (I) and the anions X, Y, Z,…on the second sublattice (II). In quadruplet approximation, the model takes into account simultaneously the first-nearest neighbour (FNN) interactions between sublattices and the second-nearest neighbour (SNN) interactions within a sublattice. Moreover, the model has been used in previous works performed at JRC and it is therefore compatible with the developed database.

The available thermodynamic database contains a large number of common-anion systems in which fluorine is the only anion present on the second sublattice. According to the model, the liquid solution for these systems is defined by the formation of the generic second-nearest neighbour pair $(A-F-B)$ as given by the following reaction:

$$(A-F-A) + (B-F-B) = 2(A-F-B) \qquad \Delta g_{AB/F} \qquad (2)$$

where $\Delta g_{AB/F}$ is the Gibbs energy change related to the pair formation and it is an empirical parameter of the model.

In the present work, a second anion (iodine) is present on sublattice II. Therefore, the distribution of the generic quadruplets ABX_2, A_2XY and ABXY must be considered and represent respectively the case of a common-anion system, a common-cation system and a mixed system. The quadruplet formation is given by the following reactions:

$$(A_2X_2)_{quad} + (B_2X_2)_{quad} = 2(ABX_2)_{quad} \qquad \Delta g_{AB/X_2} \qquad (3)$$

$$(A_2X_2)_{quad} + (A_2Y_2)_{quad} = 2(A_2XY)_{quad} \qquad \Delta g_{A_2/XY} \qquad (4)$$

$$\frac{1}{2}(ABX_2 + ABY_2 + A_2XY + B_2XY) = 2(ABXY) \qquad \Delta g_{AB/XY} \qquad (5)$$

where $\Delta g_{AB/X_2}$, $\Delta g_{A_2/XY}$ and $\Delta g_{AB/XY}$ are the Gibbs energy change related to the quadruplet formation and are also empirical parameters of the model. It is important to mention that the parameter $\Delta g_{AB/X_2}$ in the A,B,C…//X subsystem is identical to the parameter $\Delta g_{AB/X}$ for pair approximation in Equation (2).

The Gibbs energy change terms can be expanded in polynomial form such as:

Table 3
The thermodynamic data $\Delta_f H^{298}$ (kJ·mol^{-1}), S^{298} (J·K^{-1}·mol^{-1}) and C_P(J·K^{-1}·mol^{-1}) for pure compounds and intermediate compounds used in this study.

Compound	$\Delta_f H^{298}$	S^{298}	C_P				Ref.
			a	b·T	c·T^2	d·T^{-2}	
LiF (cr)	−616.931	35.66	43.309	$1.631.10^{-2}$	$5.047.10^{-7}$	$-5.691.10^{5}$	[5]
LiF (l)	−598.654	42.96	64.183				[5]
ThF_4(cr)	−2097.900	142.05	122.173	$8.37.10^{-3}$		$-1.255.10^{6}$	[4]
ThF_4(l)	−2103.654	101.24	170.0				[4]
CsF (cr)	−554.673	93.6	24.291	$6.46.10^{-2}$		$5.900.10^{5}$	[9]
CsF (l)	−534.714	108.19	70.56				[9]
CsI (cr)	−348.100	122.2	43.815	$2.184.10^{-2}$	$2.496.10^{-6}$	$2.002.10^{5}$	[6]
CsI (l)	−311.911	131.89	74.268				[6]
LiI (cr)[a]	−270.077	85.77	99.134	$-1.830.10^{-1}$	$2.730.10^{-4}$	$-1.394.10^{6}$	[5]
LiI (l)	−258.349	98.61	63.178				[5]
ThI_4 (cr)	−669.600	251.0	140	$1.35\ .10^{-2}$		$-6.15\ .10^{5}$	[7]
ThI_4 (l)	−638.248	275.24	176				[7]
$LiThF_5$(cr)	−2719.490	181.89	165.482	$2.468.10^{-2}$	$5.047.10^{-7}$	$-1.824.10^{6}$	[4]
Li_3ThF_7(cr)	−3960.259	236.1	282.100	$5.730.10^{-2}$	$1.514.10^{-6}$	$-2.962.10^{6}$	[4]
$LiTh_2F_9$(cr)	−4822.329	324.29	287.655	$3.305.10^{-2}$	$5.047.10^{-7}$	$-3.079.10^{6}$	[4]
$LiTh_4F_{17}$(cr)	−9021.140	609.0	532.001	$4.979.10^{-2}$	$5.047.10^{-7}$	$-5.589.10^{6}$	[4]
Cs_3ThF_7 (cr)	−3870.476	456.00	195.05	$2.022.10^{-1}$		$5.149.10^{5}$	[10]
Cs_2ThF_6(cr)	−3269.400	372.40	170.76	$1.376.10^{-1}$		$-7.504.10^{4}$	[10]
α-$CsThF_5$(cr)	−2722.900	225.20	146.46	$7.300.10^{-2}$		$-6.650.10^{5}$	[10]
β-$CsThF_5$(cr)	−2710.900	237.94	146.46	$7.300.10^{-2}$		$-6.650.10^{5}$	[10]
$Cs_2Th_3F_{14}$(cr)	−7555.000	593.00	415.10	$1.543.10^{-1}$		$-2.585.10^{-6}$	[10]
$CsTh_2F_9$(cr)	−4818.625	376.57	268.64	$8.135.10^{-2}$		$-1.920.10^{6}$	[10]
$CsTh_3F_{13}$(cr)	−6940.048	501.14	390.81	$8.972.10^{-2}$		$-3.175.10^{6}$	[10]
$CsTh_6F_{25}$(cr)	−13230.900	939.42	757.33	$1.148.10^{-1}$		$-6.940.10^{6}$	[10]
$LiCsF_2$ (cr)	−1174.578	129.8	67.600	$8.091.10^{-2}$	$5.047.10^{-7}$	$2.085.10^{4}$	this work
Cs_2ThI_6 (cr)	−1383.300	495.4	227.63	$5.718.10^{-2}$	$4.992.10^{-6}$	$-2.145.10^{5}$	this work
$LiThI_5$(cr)[b]	−944.336	336.772	178.81	$4.687.10^{-2}$	$3.562.10^{-8}$	$-4.892.10^{5}$	this work
Li_3ThI_7(cr)[c]	−1491.396	508.32	256.44	$1.136.10^{-1}$	$1.068.10^{-7}$	$-2.377.10^{5}$	this work
$LiTh_2I_9$(cr)[d]	−1618.875	587.772	318.81	$6.037.10^{-2}$	$3.562.10^{-8}$	$-1.104.10^{6}$	this work
$LiTh_4I_{17}$(cr)[e]	−2961.086	1089.77	598.81	$8.737.10^{-2}$	$3.562.10^{-8}$	$-2.334.10^{6}$	this work

[a] Additional terms: $-1.156\cdot10^{-7}\,\mathbf{T}^3$.
[b] In the T range 839 K–1000 K: C_p (J·K^{-1}·mol^{-1}) = 189.27 + $3.337\cdot10^{-2}\mathbf{T}$ + $3.562.10^{-8}\,\mathbf{T}^2$ + $1.258.10^{5}\,\mathbf{T}^{-2}$ and in the T range 1000–2500 K: C_p (J·K^{-1}·mol^{-1}) = 226.64.
[c] In the T range 839 K–1000 K: C_p (J·K^{-1}·mol^{-1}) = 266.90 + $1.100.10^{-1}\mathbf{T}$ + $1.068.10^{-7}\,\mathbf{T}^2$ + $3.773.10^{5}\,\mathbf{T}^{-2}$ and in the T range 1000–2500 K: C_p (J·K^{-1}·mol^{-1}) = 379.03.
[d] In the T range 839 K–1000 K: C_p (J·K^{-1}·mol^{-1}) = 339.72 + $3.337.10^{-2}\mathbf{T}$ + $3.562.10^{-8}\,\mathbf{T}^2$ + $1.258.10^{5}\,\mathbf{T}^{-2}$ and in the T range 1000–2500 K: C_p (J·K^{-1}·mol^{-1}) = 377.09.
[e] In the T range 839 K–1000 K: C_p (J·K^{-1}·mol^{-1}) = 640.63 + $3.337.10^{-2}\mathbf{T}$ + $3.562.10^{-8}\,\mathbf{T}^2$ + $1.258.10^{5}\,\mathbf{T}^{-2}$ and in the T range 1000–2500 K: C_p (J·K^{-1}·mol^{-1}) = 678.00.

Table 4
The thermodynamic data $\Delta_f H^{298}$ (kJ·mol^{-1}), S^{298} (J·K^{-1}·mol^{-1}) and C_P(J·K^{-1}·mol^{-1}) for the gaseous species considered in this study.

Compound	$\Delta_f H^{298}$	S^{298}	C_P				T range	Ref.
			a	b·T	c·T^2	d·T^{-2}		
LiF(g)	−340.946	200.19	35.398	$1.871.10^{-3}$	$-1.654.10^{-7}$		298.15–6000 K	[5]
Li_2F_2(g)	−935.323	261.80	83.094	$1.000.10^{-5}$		$-2.17.10^{6}$	298.15–6000 K	[5]
Li_3F_3(g)	−1524.598	316.70	132.924	$3.000.10^{-5}$		$-3.75.10^{6}$	298.15–6000 K	[5]
ThF_4(g)[a]	−1748.200	351.56	122.407	$-1.406.10^{-2}$	$7.365.10^{-6}$		298.15–6000 K	[11]
CsF(g)	−356.500	243.21	37.386	$5.70.10^{-4}$		$-1.571.10^{5}$	298.15–6000 K	[5]
CsI(g)	−153.300	275.17	37.886	$3.058.10^{-5}$	$4.913.10^{-7}$	$-4.535.10^{-4}$	298.15–3000 K	[6,12]
			−34.730	$2.842.10^{-2}$	$-2.572\ .10^{-6}$	$1.362.10^{8}$	3000–6000 K	[6,12]
Cs_2I_2(g)	−469.200	431.29	83.143	$6.384.10^{-7}$	$-8.053.10^{-11}$	$-4.147.10^{4}$	298.15–6000 K	[6,12]
LiI(g)	−91.002	232.26	37.223	$8.057.10^{-4}$	$-1.179.10^{-8}$	$-2.647.10^{5}$	298.15–6000 K	[5]
Li_2I_2(g)	−361.920	330.61	82.952	$9.877.10^{-5}$	$-1.195.10^{-8}$	$-6.248.10^{-5}$	298.15–6000 K	[5]
Li_3I_3(g)	−612.458	425.17	129.989	$5.414.10^{-3}$	$-2.682.10^{-6}$	$-8.686.10^{-5}$	298.15–1000 K	[13]
			133.026			$-1.162.10^{-6}$	1000–3000 K	[13]
ThI_4(g)	−460.600	478.5	100.492	$2.102.10^{-2}$	$-1.365.10^{-5}$	$6.636.10^{4}$	298.15–2000 K	[13]
			108.961	$1.004.10^{-3}$	$-1.397\ .10^{-7}$	$-4.096.10^{5}$	600–2000 K	[13]
ThI_3(g)	−187.443	429.84	82.885	$6.320.10^{-4}$	$-4.100.10^{-7}$	$-1.100.10^{5}$	298.15–1000 K	[13]
			83.341	$-1.300.10^{-4}$	$2.500.10^{-8}$	$-2.732.10^{5}$	1000–3000 K	[13]
ThI_2(g)	61.505	355.48	58.137	$1.300.10^{-4}$	$-7.500.10^{-8}$	$-7.030.10^{4}$	298.15–1000 K	[13]
			58.199	$4.000.10^{-6}$		$-7.610.10^{-4}$	1000–3000 K	[13]
ThI(g)	348.109	288.49	37.408	$1.530.10^{-3}$	$6.890.10^{-7}$	$-3.140.10^{-4}$	298.15–2500 K	[13]

[a] Additional terms: $-1.939.10^{-9}\mathbf{T}^3$ + $2.011.10^{-13}\mathbf{T}^4$ - 7544.56·$\mathbf{T}^{-1}$.

$$\Delta g_{AB/X_2} = \Delta g^{0}_{AB/X_2} + \sum_{i\geqq 1} g^{i0}_{AB/X_2}\chi^{i}_{AB/X_2} + \sum_{j\geqq 1} g^{0j}_{AB/X_2}\chi^{j}_{BA/X_2} \quad (6)$$

$$\Delta g_{A_2/XY} = \Delta g^{0}_{A_2/XY} + \sum_{i\geqq 1} g^{i0}_{A_2/XY}\chi^{i}_{A_2/XY} + \sum_{j\geqq 1} g^{0j}_{A_2/XY}\chi^{j}_{A_2/YX} \quad (7)$$

$$\Delta g_{AB/XY} = \Delta g^{0}_{AB/XY} + \sum_{i\geq 1}\left(g^{i}_{AB/XY(AX)}\chi^{i}_{A_2/X_2} + g^{i}_{AB/XY(BX)}\chi^{i}_{B_2/X_2} + g^{i}_{AB/XY(AY)}\chi^{i}_{A_2/Y_2} + g^{i}_{AB/XY(AX)}\chi^{i}_{A_2/X_2}\right) \quad (8)$$

where $\Delta g^{0}_{AB/XY}$ and $g^{ij}_{AB/XY}$ are composition independent coefficients while the dependence of the parameter on composition is given by the quadruplet fractions $\chi_{AB/XY}$.

Finally, the charge-neutrality condition for the ABXY quadruplets in a molten fluoride salt solution must be fulfilled and it is done by the definition of the coordination numbers respecting the absolute cationic and anionic charges ($q_A, q_B, \ldots$):

$$\frac{q_A}{Z^{A}_{AB/XY}} + \frac{q_B}{Z^{B}_{AB/XY}} = \frac{q_F}{Z^{X}_{AB/XY}} + \frac{q_F}{Z^{Y}_{AB/XY}}. \quad (9)$$

In this work, the cation-cation coordination numbers were set to 6.0 as default value, except for $Z^{Li}_{LiTh/jj}$(j = F, I) which were set to 2.0 and $Z^{Cs}_{CsTh/jj}$(j = F, I) which were set to 3.0. For these systems, different cation-cation coordination numbers were selected during the assessment to better represent the composition of short range ordering (see details in the works [4,10]).

The optimized common-ion binary parameters for the liquid solution as used in this work are given below (J · mol^{-1}):

$$\Delta g_{LiTh/F_2} = -10883 + \chi_{LiTh/F_2}(-6697 + 2.93\,T) + \chi_{ThLi/F_2}(-20930 + 19.25\,T) \quad (10)$$

$$\Delta g_{CsTh/F_2} = -39329.6 - 11234\,\chi_{CsTh/F_2} + 2928.8\chi_{ThCs/F_2} \quad (11)$$

$$\Delta g_{LiCs/F_2} = -5039 + 1374.86\chi_{CsLi/F_2} \quad (12)$$

$$\Delta g_{Cs_2/FI} = -2540 + 500\chi_{Cs_2/FI} \quad (13)$$

$$\Delta g_{Li_2/FI} = -1434 + 2\,T + \chi_{Li_2/FI}(3.0\,T) \quad (14)$$

$$\Delta g_{LiCs/I_2} = -5600 - 2300\chi_{LiCs/I_2} \quad (15)$$

$$\Delta g_{CsTh/I_2} = -5228 - 8300\,\chi_{ThCs/I_2} \quad (16)$$

$$\Delta g_{Th_2/FI} = -1384 \quad (17)$$

$$\Delta g_{LiTh/I_2} = -10883 + \chi_{LiTh/I_2}(-6697 + 2.93\,T) + \chi_{ThLi/I_2}(-20930 + 19.25\,T) \quad (18)$$

Using the data of the binary phase diagrams, the common-ion ternary phase diagrams and the reciprocal systems have been extrapolated using the Kohler or the Kohler/Toop interpolation methods depending on the symmetric or asymmetric nature of the system. In this case, ThF_4 and ThI_4 are considered as asymmetric components as their chemical behaviour and their ionic nature is different compared to the alkali halides. Some ternary parameters (Δg^{ijk}_{ABC}) and reciprocal terms ($\Delta g^{0}_{AB|XY}$) have been introduced to optimize the phase diagrams according to the experimental data:

$$\Delta g^{001}_{LiTh(Cs)|FF} = 4000 \quad \text{J·mol}^{-1} \quad (19)$$

$$\Delta g^{0}_{LiCs|FI} = -600 \quad \text{J·mol}^{-1} \quad (20)$$

4. Results

4.1. Common ion binary subsystems

All the common-ion binary subsystems have been reviewed in this work as they are essential for the extrapolation to higher order systems. The binary LiF-ThF_4 and CsF-ThF_4 systems have been already extensively described in previous works [10,15] and the same liquid model parameters as reported in these publications were considered in the present work. The assessment of the remaining systems is described in this section.

4.1.1. The LiF-CsF and the CsF-CsI systems

Slight adjustments have been made for the LiF-CsF and CsF-CsI systems due to the recent re-assessment of the thermodynamic properties of both the solid and liquid phase of CsF [9]. Although there is no qualitative difference for the calculated phase diagrams compared to the previous assessments, slightly different parameters were used to optimize the liquid solution and the intermediate compounds. The calculated phase diagram for the LiF-CsF system is shown in Fig. 1 along with all the experimental data used for the assessment [16–18]. The system is characterized by one eutectic point at T = 758.1 K and X_{CsF} = 0.59 mol% and one peritectic point at T = 765.7 K and X_{CsF} = 0.48 mol%, in agreement with the previously published works [19,20].

Similarly, the binary CsF-CsI system has been re-optimized in the present work. As shown in Fig. 2, one single eutectic characterizes the system and it is found at 704.3 K and X_{CsI} = 0.53 mol%. While experimental data on the liquidus line of the CsF-CsI system have been measured by Bukhalova et al. [21], no data were available for the solidus line. In order to confirm the eutectic temperature and the general shape of the phase diagram, new phase equilibria data have been measured in this work using the DSC technique. Three selected compositions (X_{CsI}=0.26 mol%; 0.53 mol%; and the 0.76 mol%) have been measured and the results are reported in Table 5. The eutectic temperature was confirmed experimentally (T = 706.8 K) and the measured liquidus temperatures agree well with the model and the literature data.

4.1.2. The LiI-LiF and the LiI-CsI systems

The calculated phase diagrams of the LiI-LiF and the LiI-CsI systems are shown in Fig. 3 and Fig. 4, respectively. The LiI-LiF system was assessed based on the literature data from Johnson and Hathaway [22], who measured the phase equilibria of several selected compositions. One eutectic point was found at T = 688.5 K for the composition X_{LiI} = 0.83 mol%. On the contrary, there are no experimental reports on the phase diagram of the LiI-CsI system, which was assessed based on the enthalpy of mixing data of the (Li_x, Cs_{1-x})I liquid solution [23]. The eutectic point is predicted at T = 446.3 K for the composition X_{LiI} = 0.62 mol%. While the calculated eutectic point of the LiI-LiF system agree well with the evaluation of Sangster [19], a lower eutectic temperature was found for the LiI-CsI system most likely due to the use of different thermodynamic properties for the end-members.

4.1.3. The CsI-ThI_4, LiI-ThI_4, and ThI_4-ThF_4 systems

Very little information is available for the ThI_4-containing systems. Brendel et al. [24] reported the stability of the intermediate compound Cs_2ThI_6 and showed the DTA curve at this exact composition. The eutectic temperature of the CsI-ThI_4 mixture was

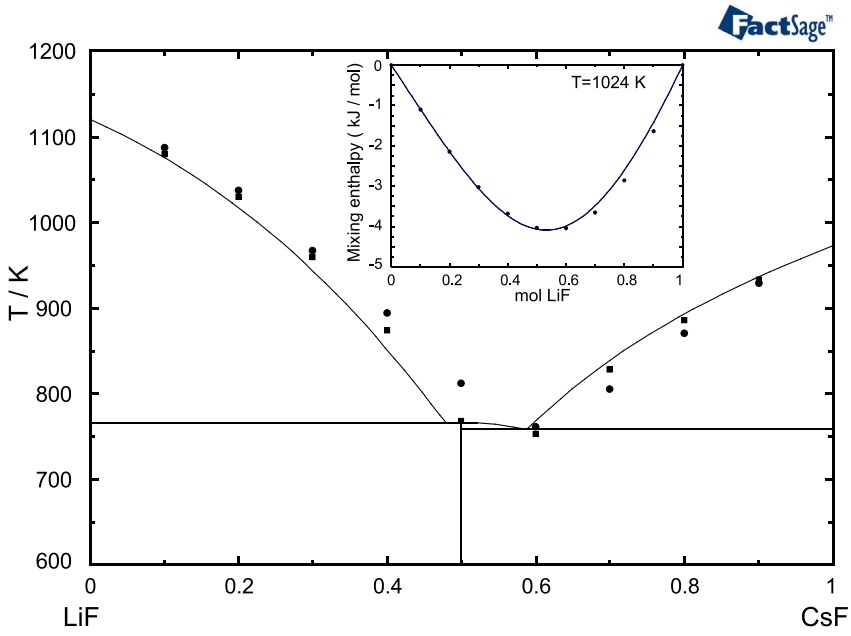

Fig. 1. Phase diagram of the LiF-CsF system. • Data by Bukhalova and Sementsova [16]. ■ Data by Thoma [17]. Inset graph: Enthalpy of mixing of the $(Li_x, Cs_{1-x})F$ liquid solution at 1024 K. The solid line corresponds to the calculated value from the model while the black points are the experimental data from Ref. [18].

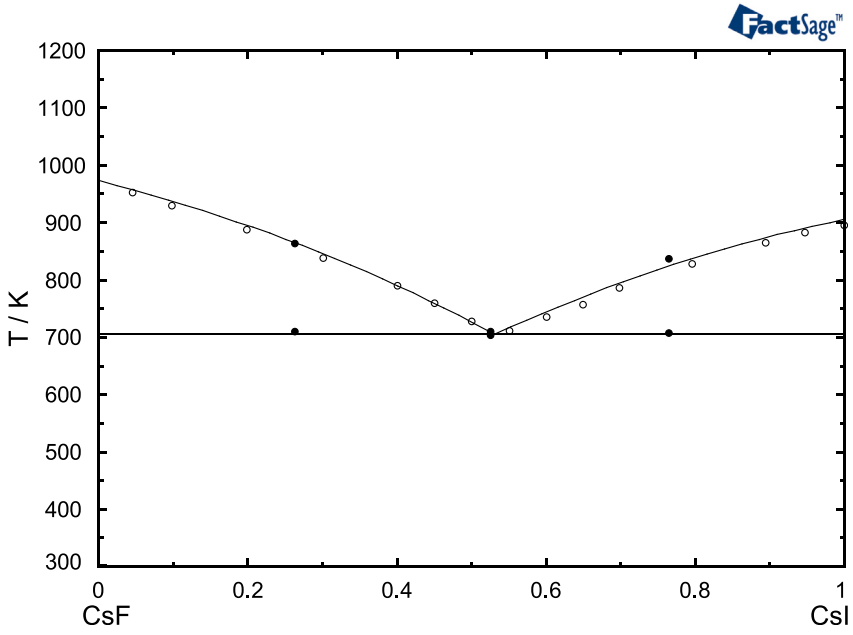

Fig. 2. Phase diagram of the CsF-CsI system. ◦ Data by Bukhalova et al. [21]. • Data measured in this work.

found at 728 K and the formation of the intermediate compound was found at 803 K. Based on these very limited information, a phase diagram for the CsI-ThI_4 is proposed and shown in Fig. 5. The eutectic point was found at T = 728.1 K for the composition $X_{ThI_4} = 0.62$ mol% while the peritectic point was found at T = 802.8 K for the composition $X_{ThI_4} = 0.27$ mol%.

No data were found in literature for the ThF_4-ThI_4 and the LiI-ThI_4 systems, thus no direct optimization of the phase diagrams was possible. Although for the calculation of cesium and iodine behaviour in MSR the description of these systems has a limited influence, an effort was made to go beyond the ideal solution treatment. The proposed phase diagrams are based on the similarities with the related binary systems assessed in this work from which the liquid excess parameters were taken.

All the common-cation systems evaluated in the present work (LiF-LiI, CsF-CsI) are eutectic systems with no solid solubility and no intermediate compounds. Therefore, a similar behaviour is reasonably expected for the ThF_4-ThI_4 system. Fig. 6 shows the calculated phase diagrams of the ThF_4-ThI_4 system when the liquid excess parameters as assessed for LiF-LiI and the CsF-CsI systems, respectively, are used. The eutectic temperatures obtained are close to each other and the selected phase diagram, indicated with a solid line, is calculated using an average of the two liquid solution data. The eutectic is found at 543 K with a maximum probable

Table 5
The phase equilibria of the selected composition measured in this work using the DSC technique.

System	X_{LiF}	X_{CsF}	X_{ThF_4}	X_{CsI}	T/K	Type of equilibrium
CsF-CsI	–	0.235	–	0.765	706.2	Eutectic
	–		–		835.2	Liquidus
	–	0.737	–	0.263	708.1	Eutectic
					862.7	Liquidus
	–	0.474	–	0.526	706.3	Eutectic
					709.1	Liquidus
LiF-CsF-ThF_4	0.366	0.612	0.022	–	750.2	Eutectic
LiF-CsI	0.957	–	–	0.043	898.0	CsI stability limit
					1119.9	Lower limit miscibility gap
					1131.0[a]	LiF stability limit
					1550.6	Upper limit miscibility gap
	0.808	–	–	0.192	891.3	CsI stability limit
					1112.9	Lower limit miscibility gap
					1115.6[a]	LiF stability limit
	0.019	–	–	0.981	899.9	CsI stability limit
					1114.3	Upper limit miscibility gap
LiF-CsF-CsI	0.331	0.603	–	0.066	716.2	Eutectic
					761.5	Peritectic
ThF_4-CsI		–	0.976	0.024	843.8	CsI stability limit
					1302.2	Lower limit miscibility gap
					1366.6	Upper limit miscibility gap
		–	0.954	0.046	1299.5	Lower limit miscibility gap
					1315.6	ThF_4 stability limit
					1348.8	Upper limit miscibility gap
		–	0.919	0.081	843.6	CsI stability limit
					1305.8	Lower limit miscibility gap
					1355.8	ThF_4 stability limit
					1384.4	Upper limit miscibility gap
		–	0.592	0.408	882.4	CsI stability limit
					1318.1	Lower limit miscibility gap
					1362.6	ThF_4 stability limit

[a] Temperature determined solely from the cooling curves.

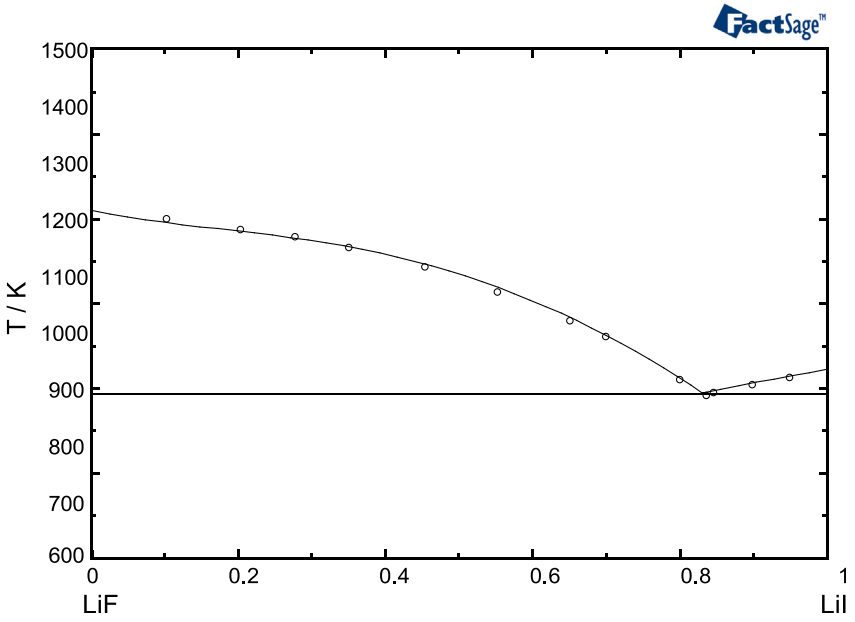

Fig. 3. Phase diagram of the LiI-LiF system assessed in this study. ◦ Data by Johnson and Hathaway [22].

temperature inaccuracy of ±50 K, based on phase diagrams comparison.

In case of the LiI-ThI_4 systems, the same excess parameters as optimized in Ref. [15] for the LiF-ThF_4 were considered. Moreover, four intermediate compounds with similar stoichiometry to the fluoride system were supposed to be present also for the iodide system. The thermodynamic properties of the compounds were estimated based on the weighted average from the properties of their end-members and adding an enthalpy contribution related to the compounds formation reaction (same as in LiF-ThF_4

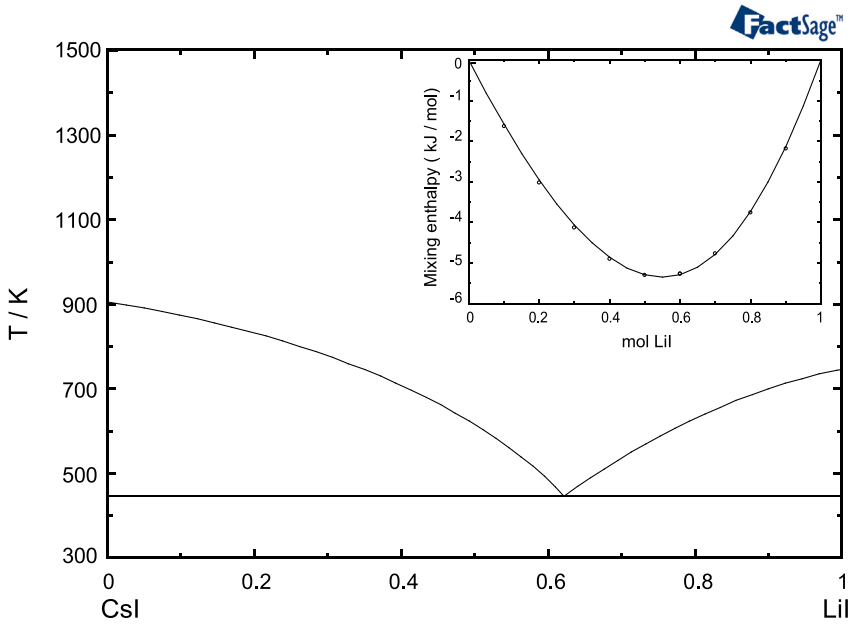

Fig. 4. Phase diagram of the LiI-CsI system assessed in this study. Inset graph: Enthalpy of mixing of the $(Li_x, Cs_{1-x})I$ liquid solution at 1013 K • Data by Melnichak and Kleppa [23].

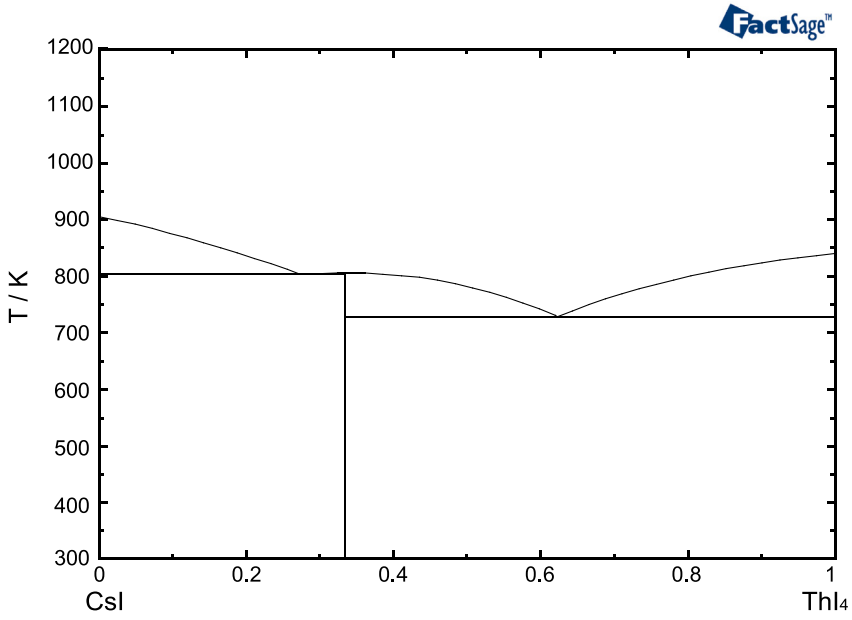

Fig. 5. Phase diagram of the CsI-ThI_4 system.

system). A tentative phase diagram is shown in Fig. 7 and is compared with the ideal behaviour (no interactions and no intermediate compounds). Given the large deviation in terms of the eutectic temperature and in order to confirm the validity of the assumptions, the same approach was tested on the LiCl-$ThCl_4$ system for which the eutectic temperature is known [25]. The predicted eutectic temperature of 703 K compares well with the literature value of 681 K considering the uncertainties of the estimation method.

Further investigations for all the binary systems in this section are recommended to confirm the shape of the phase diagrams and, more importantly, the temperature and the composition of the invariant points. This requires novel experimental data on the phase equilibria and the excess properties.

4.2. Common-ion ternary subsystems

Two common-ion ternary subsystems, i.e. the LiF-CsF-ThF_4 and the LiI-CsI-ThI_4 systems, can be calculated based on the binary phase diagrams described above. No ternary interactions were considered for the iodide systems, as no data were found in literature, and is therefore not discussed further here.

4.2.1. The LiF-CsF-ThF_4 system

The ternary LiF-CsF-ThF_4 phase diagram was extrapolated based on the assessed binary phase diagrams according to the Kohler/Toop formalism without any additional ternary compound. A small ternary parameter was introduced to reproduce the partial pressure of CsF in the ternary mixture LiF-CsF-ThF_4

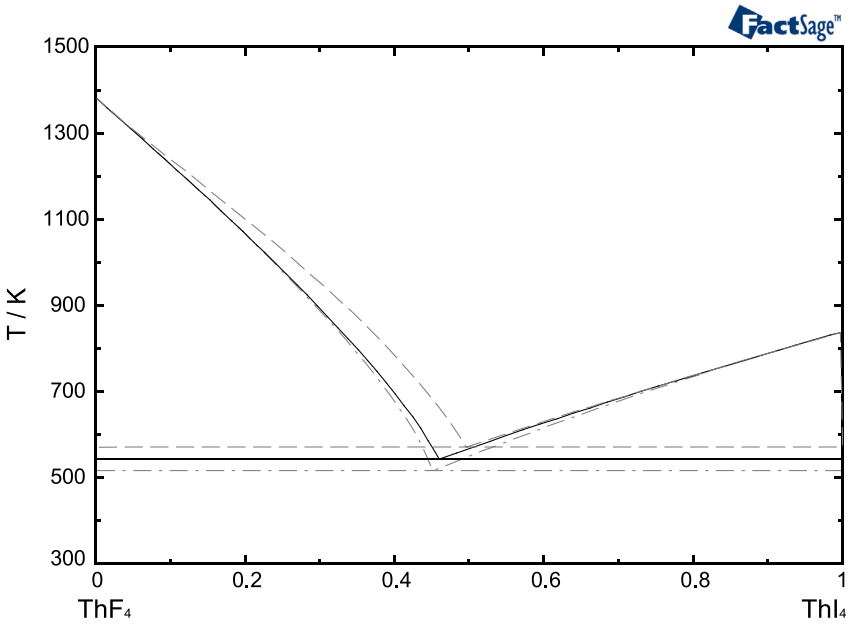

Fig. 6. Phase diagram of the ThF_4-ThI_4 system estimated in this work. Dashed line: phase diagram calculated based on the LiF-LiI liquid excess parameters. Dashed-dotted line: phase diagram calculated based on the CsF-CsI liquid excess parameters.

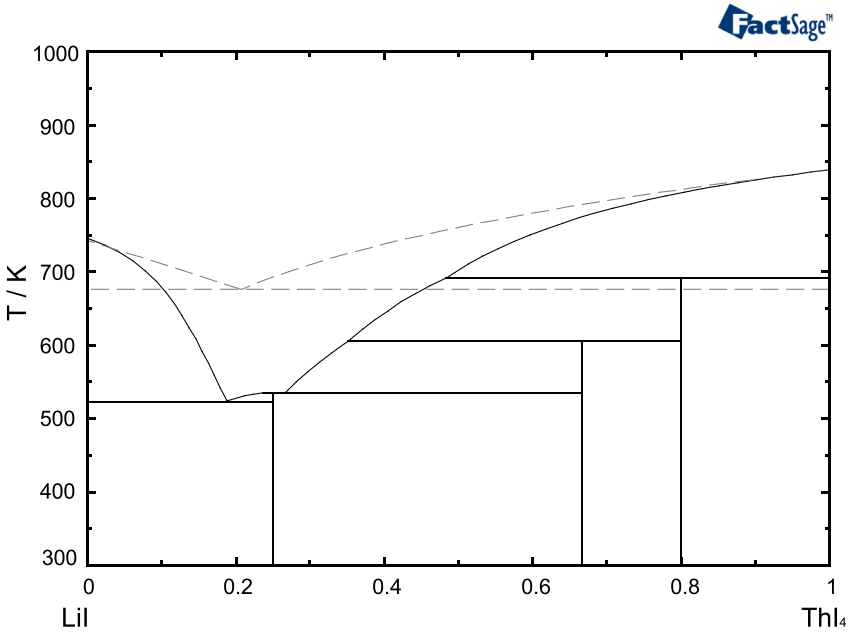

Fig. 7. Phase diagram of the LiI-ThI_4 system estimated in this work. Dashed line: Ideal behaviour without intermediate compounds.

(75.73-23.23-1.05) measured in Ref. [26] and shown in Fig. 8. The calculated liquidus projection of the LiF-CsF-ThF_4 system is shown in Fig. 9 with indicated primary crystallization fields. In total, sixteen invariant points and three saddle points were identified and are listed in Table 6. The extrapolation was confirmed by the experimental determination of one of the eutectic points (temperature and composition) in the system. The experimental eutectic temperature was found at 750.2 K for a synthesized composition of LiF-CsF-ThF_4 (36.6-61.2-2.2 mol%) and compares very well with the calculated temperature of 748.3 K for the composition LiF-CsF-ThF_4 (35.3-61.4-3.3 mol%).

4.3. The Li,Cs//F,I reciprocal system

The only available data for the Li,Cs//F,I reciprocal system were reported by Dvoryanova et al. [27,28]. They are mostly estimates based on the regularities in the structure of the liquidus surfaces of systems with the presence of fluoride-halide exchange. Margheritis et al. [29] observed the occurence of a miscibility gap in the series of fused systems LiF-AlkX (Alk = Na, K, Rb, Cs; X = Cl,Br,I) with an increasing tendency to demix as the radius of the alkali cation and the halide anion increases. The LiF-CsI system was found to have the broadest liquid-liquid miscibility gap which extends over

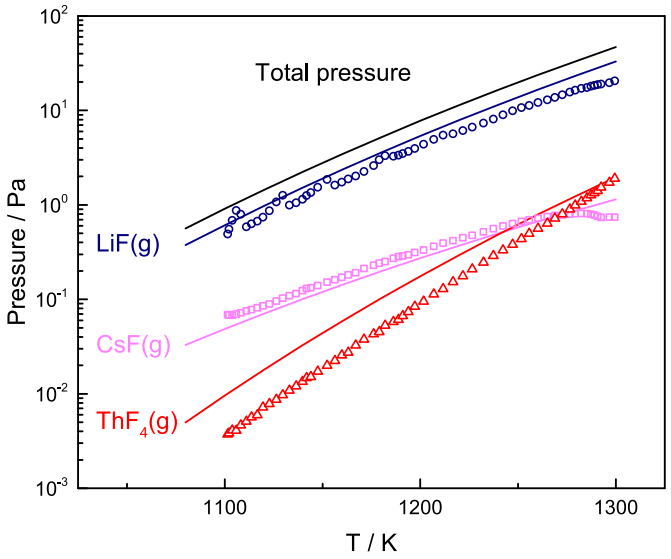

Fig. 8. The comparison between the calculated and experimental vapor pressure of the LiF-ThF_4-CsF (75.73-23.23-1.05) mixture. Black line: total pressure over the ternary salt. Blue line and symbols (◦): Data for LiF(g). Pink line and symbols (□): Data for CsF(g). Red line and symbols (△): Data for ThF_4(g). (For interpretation of the references to colour in this figure legend, the reader is referred to the Web version of this article.)

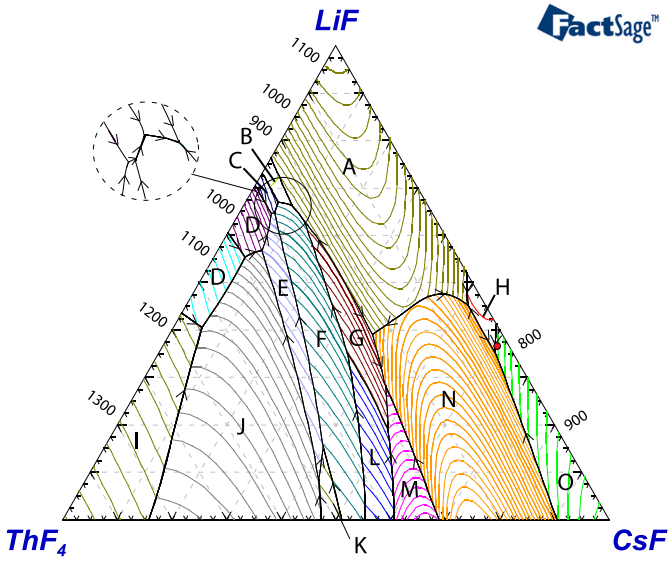

Fig. 9. The liquidus projection of the calculated LiF-ThF_4-CsF system. Primary crystallization fields: (A) LiF; (B) Li_3ThF_7; (C) $LiThF_5$; (D) $LiTh_2F_9$; (E) $CsTh_3F_{13}$; (F) $Cs_2Th_3F_{14}$; (G) α-$CsThF_5$; (H) $LiCsF_2$; (I) ThF_4; (J) $CsTh_6F_{25}$; (K) $CsTh_2F_9$; (L) β-$CsThF_5$; (M) Cs_2ThF_6; (N) Cs_3ThF_7; (O) CsF.

almost the entire composition range.

In order to complement the existing literature data, the LiF-CsI join has been experimentally investigated in the present work. The phase equilibria of three selected compositions were measured using the DSC technique and the obtained data, reported in Table 5, were used to assess the Li,Cs//F,I reciprocal system. The experimental results, and in particular the range of stability of the liquid-liquid miscibility gap, were correctly reproduced introducing a small ternary parameter, as shown in Fig. 10. Since CsI vaporizes (T_{boil} = 1553 K) at temperatures close to the measurement upper limit, the gaseous phase was included in the calculations and is shown in the phase diagram. As mentioned before, the higher evaporation of CsI in comparison with LiF might cause a slight change in the sample composition during the measurements. This effect clearly occurred for one of the samples (X_{CsI} = 4 mol%) for which a temperature decrease was observed for the liquidus transition in the subsequent cycles. The temperature change is consistent with a shift of 0.5 mol% and only the data measured during the first cycle were considered in the optimization. Two of the observed transitions, namely the lower limit of the miscibility gap and the LiF stability limit, are very close in temperature and could not be distinguished upon heating. However, the cooling curve shows two separate peaks and the transition temperatures were determined by extrapolation to zero of the onset temperature measured at different cooling rates.

One composition ternary composition was also measured outside the LiF-CsI join, close to the peritectic point in the LiF-CsF-CsI system (exact composition in Table 5). The temperatures measured, T = 716.2 K and 761.5 K, agree rather well with the calculated temperatures (T = 703.1 K and T = 750.5 K), validating the predictive ability of the thermodynamic assessment.

The calculated liquidus projection of the Li,Cs//F,I system is shown in Fig. 11. As expected, the phase field of LiF, which is the highest melting component, is predominant and a liquid-liquid miscibility gap is calculated along the LiF-CsI join for temperatures above 1115 K. The system exhibit a strong FNN SRO so that the Li-F and Cs-I nearest neighbour pairs predominate. Seven invariant equilibria were found for this system and are reported in Table 7.

4.4. The Cs,Th//F,I reciprocal system

No reported liquidus projection has been found in literature for the Cs,Th//F,I system. Following the approach adopted for the Li,Cs//F,I system, novel experimental data were measured for compositions along the ThF_4-CsI join. The experimental phase equilibria are reported in Table 5 and were correctly reproduced (Fig. 12) by the thermodynamic model with no additional reciprocal parameters. The larger discrepancy was observed for the transition at 905 K, corresponding to the CsI stability limit. The peak registered at this temperature was small and very broad, especially for low CsI concentrations, and thus the determination of the onset point has a higher uncertainty.

The calculated liquidus projection of the Th,Cs//F,I system is shown in Fig. 13 and the invariant equilibria are reported in Table 8. Also in this case, the system show a strong short range order and the ThF_4 phase field predominates.

4.5. The Li,Th//F,I reciprocal system

The last reciprocal system of the series, the Li,Th//F,I system, was calculated assuming no ternary reciprocal parameters and it is shown in Fig. 14. The invariant point of the system are also reported in Table 9. The system shows a less pronounced SRO character, which is consistent with the Gibbs energy exchange calculated in Section 3.1 and no liquid-liquid miscibility gap.

5. Cesium and iodine behaviour in the fuel mixture

The main result of the thermodynamic modeling described in this work is a consistent and complete description of the Li, Th,Cs//F,I system. That implies that the thermodynamic properties of any composition having these constituents can be calculated from the model. For the present discussion, we focussed on the effect of the accumulation of cesium and iodine, in the form of CsF and CsI, in the MSFR fuel mixture. The eutectic mixture LiF-ThF_4 (76.2–23.8 mol%) is the main fuel constituent for the current designs and was taken in our calculations as representative of the

Table 6
Invariant equilibria and saddle points found in the LiF-CsF-ThF_4 system.

X_{LiF}	X_{ThF_4}	X_{CsF}	T/K	Type of equilibria	Crystal phases in equilibrium
0.406	0.543	0.052	1154.5	Quasi-Peritectic	$LiTh_4F_{17}$, $CsTh_6F_{25}$, ThF_4
0.084	0.490	0.427	1137.1	Peritectic	$CsTh_2F_9$, $CsTh_3F_{13}$, $CsTh_6F_{25}$
0.155	0.446	0.399	1101.5	Quasi-Peritectic	$CsTh_2F_9$, $Cs_2Th_3F_{14}$, $CsTh_3F_{13}$
0.554	0.389	0.056	1015.6	Quasi-Peritectic	$LiTh_2F_9$, $LiTh_4F_{17}$, $CsTh_6F_{25}$
0.568	0.351	0.080	959.8	Quasi-Peritectic	$LiTh_2F_9$, $CsTh_3F_{13}$, $CsTh_6F_{25}$
0.188	0.310	0.502	942.0	$CsThF_5$ ($\alpha \rightarrow \beta$)	Cs_2ThF_6, α-$CsThF_5$, β-$CsThF_5$
0.350	0.304	0.346	942.0	$CsThF_5$ ($\alpha \rightarrow \beta$)	$Cs_2Th_3F_{14}$, α-$CsThF_5$, $CsThF_5$-β
0.448	0.138	0.414	917.4	Saddle-point	LiF, Cs_3ThF_7
0.282	0.268	0.450	858.1	Quasi-Peritectic	Cs_2ThF_6, Cs_3ThF_7, α-$CsThF_5$
0.645	0.296	0.059	849.6	Quasi-Peritectic	$LiTh_2F_9$, $CsTh_3F_{13}$, $LiThF_5$
0.649	0.288	0.063	836.8	Quasi-Peritectic	$Cs_2Th_3F_{14}$, $CsTh_3F_{13}$, $LiThF_5$
0.534	0.233	0.233	819.1	Saddle point	LiF, α-$CsThF_5$
0.670	0.271	0.059	808.0	Quasi-Peritectic	$Cs_2Th_3F_{14}$, $LiThF_5$, Li_3ThF_7
0.631	0.243	0.126	804.9	Quasi-Peritectic	LiF, $Cs_2Th_3F_{14}$, α-$CsThF_5$
0.391	0.238	0.371	801,2	Eutectic	LiF, Cs_3ThF_7, α-$CsThF_5$
0.664	0.249	0.087	798,3	Eutectic	LiF, $Cs_2Th_3F_{14}$, Li_3ThF_7
0.429	0.033	0.538	756.4	Saddle point	$LiCsF_2$, Cs_3ThF_7
0.452	0.032	0.515	756,1	Eutectic	$LiCsF_2$, LiF, Cs_3ThF_7
0.353	0.033	0.614	748,3	Eutectic	$LiCsF_2$, CsF, Cs_3ThF_7

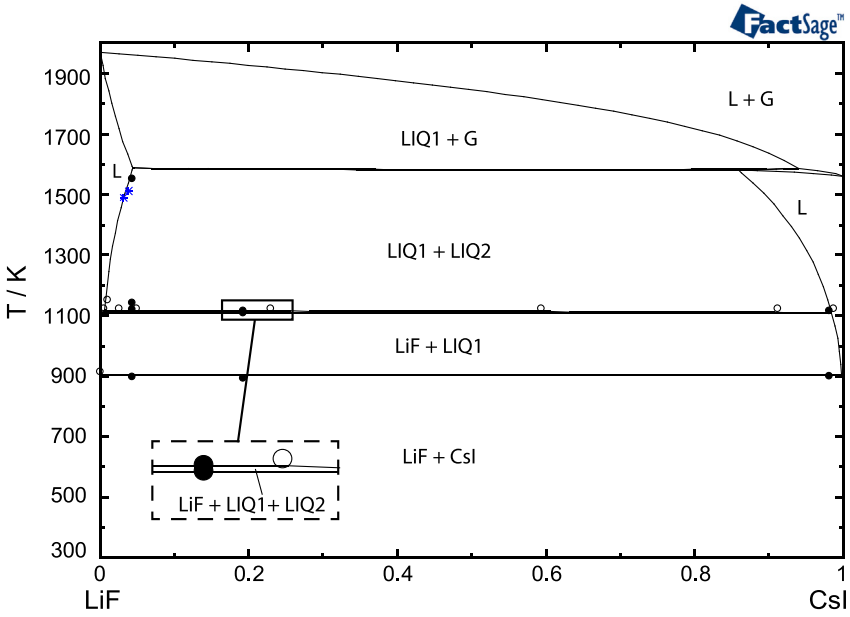

Fig. 10. The pseudo-binary phase diagram of the LiF-CsI joint. • Data measured in this work *Evolution of the liquidus point during the different cycles. ◦ Data by Margheritis et al. [29].

actual fresh fuel composition which also contains fissile in the form of UF_4 or PuF_3. The concentrations of both CsI and CsF will depend on reactor parameters and reprocessing scheme but are expected to remain below 1 mol % [30,31]. As an example, recent calculations [31] of the radionuclides inventory in MSFR reported a concentration of $4.1 \cdot 10^{-3}$ mol% for cesium at equilibrium.

In this framework, several key compositions were identified and their thermodynamic properties predicted using the model developed in this work. With regards to reactor safety, two of the most important properties of the fuel mixture are the liquidus temperature and the pressure at the reactor operation temperature. They represent the safety limit towards solidification and vaporization, respectively. In other words, the higher the liquidus temperature, the higher must be the operational temperature to ensure an adequate safety margin. The reference minimum temperature of 900 K was considered in this work based on the MSFR design ($T_{operation} \simeq$ 923–1023 K [32]), though the exact operation temperature will depend on the specific reactor design and fuel composition. The results of the thermodynamic calculations performed are reported in Table 10. For all the compositions, the molar ratio LiF/ThF_4 is kept constant and a fixed concentration of either CsF, CsI or both compounds is added.

In the form of CsF, cesium is completely soluble in the $LiF\text{-}ThF_4$ solution and there is almost no effect on the physico-chemical properties of the fuel. The liquidus temperature is unchanged for realistic CsF concentrations and at $X_{CsF} = 10$ mol% a relatively small temperature increase of 30 K is predicted. Similarly, the total vapor pressure at the reactor operation temperature slightly increases with the concentration of CsF but remains very low.

A different behaviour is observed for cesium and iodine in the

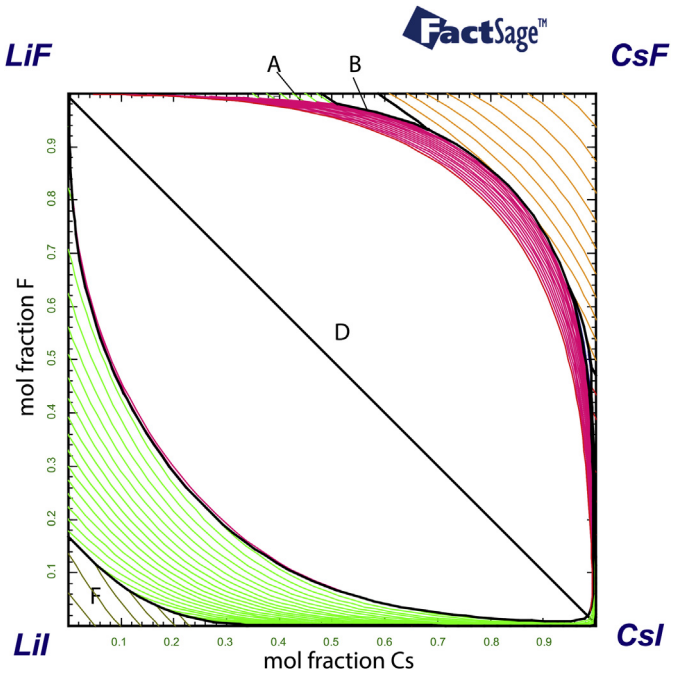

Fig. 11. The calculated liquidus projection of the Li,Cs//F,I system. Prymary crystallization fields and miscibility gap: (A) LiF; (B) $LiCsF_2$; (C) CsF; (D) liquid (miscibility gap) (E) LiI (F) CsI.

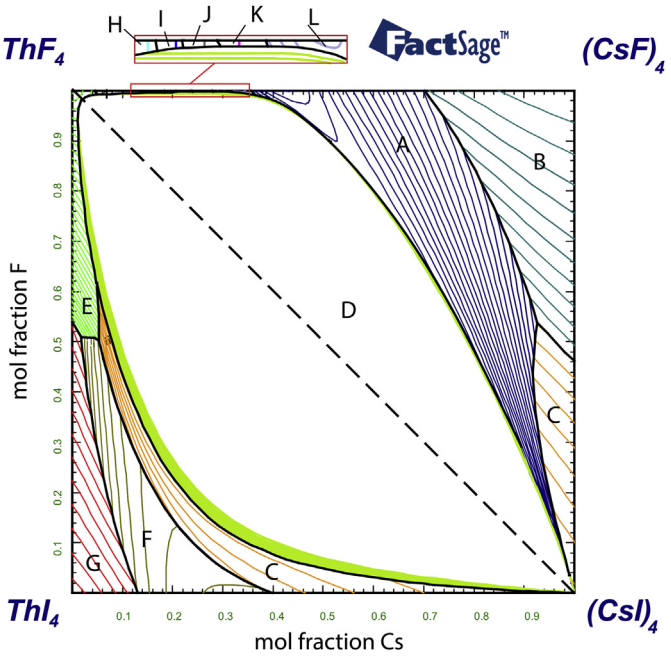

Fig. 13. The calculated liquidus projection of the Th,Cs//F,I system. Prymary crystallization fields and miscibility gap: (A) Cs_3ThF_7; (B) CsF; (C) CsI; (D) liquid (miscibility gap) (E) ThF_4 (F) Cs_2ThI_6 (G) ThI_4 (H) $CsTh_6F_{25}$ (I) $CsTh_2F_9$ (J) $Cs_2Th_3F_{14}$ (K) $CsThF_5$ (L) Cs_2ThF_6.

Table 7
Invariant equilibria found in the Li,Cs//F,I reciprocal system.

$X_{Cs/(Cs+Li)}$	$X_{F/(F+I)}$	T/K	Phases in equilibrium
0.509	0.981	762.4	LiF, $LiCsF_2$, LIQ2, LIQ1
0.989	0.426	762.3	LiF, $LiCsF_2$, LIQ2, LIQ1
0.954	0.625	749.8	CsF, $LiCsF_2$, LIQ2, LIQ1
0.677	0.936	749.8	CsF, $LiCsF_2$, LIQ2, LIQ1
0.993	0.402	748.8	LiF, $LiCsF_2$, CsI, LIQ1
0.993	0.479	703.1	CsF, $LiCsF_2$, CsI, LIQ1
0.377	0.001	446.2	LiF, CsF, CsI, LIQ1

form of CsI. The liquidus temperature increase substantially even for small concentrations of CsI (50 K at $X_{CsI} = 1$ mol%), which is a clear indication of a very limited solubility. Fig. 15 shows the calculated pseudo-binary phase diagram of the LiF-ThF_4 system with fixed concentration of CsI of 1 mol%. The main difference compared to the binary LiF-ThF_4 phase diagram is the presence of an area (shaded) corresponding to the binary eutectic in which solid CsI is present. To better understand the solubility of CsI in the fuel composition, the pseudo binary phase diagram CsI-Li_3ThF_7 was calculated and it is shown in Fig. 16. As an example, at 900 K the

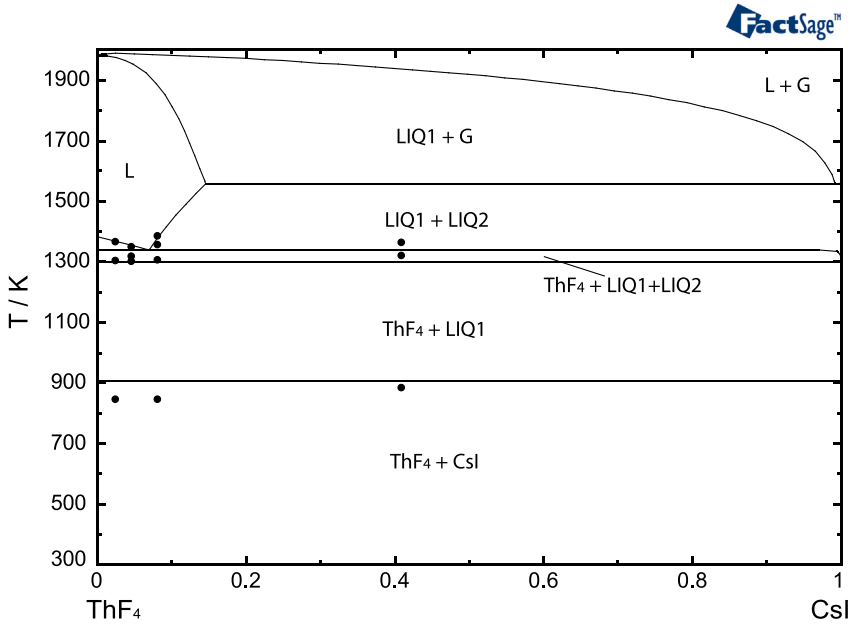

Fig. 12. The pseudo-binary phase diagram of the ThF_4-CsI joint. • Data measured in this work.

Table 8
Invariant equilibria found in the Cs,Th//F,I reciprocal system.

$X_{Cs/(Cs+4Th)}$	$X_{F/(F+I)}$	T/K	Phases in equilibrium
0.049	0.992	1305.9	$CsTh_6F_{25}$, ThF_4, LIQ2, LIQ1
0.186	0.997	1164.4	$CsTh_6F_{25}$, $CsTh_2F_9$, LIQ2, LIQ1
0.209	0.997	1140.2	$CsTh_2F_9$, $Cs_2Th_3F_{14}$, LIQ1, LIQ2
0.365	0.992	1121.8	Cs_2ThF_6, Cs_3ThF_7, LIQ2, LIQ1
0.239	0.998	1111.4	$Cs_2Th_3F_{14}$, $CsThF_5$, LIQ2, LIQ1
0.281	0.998	1070.5	$CsThF_5$, Cs_2ThF_6, LIQ1, LIQ2
0.049	0.617	899.1	ThF_4, CsI, LIQ1,LIQ2
0.908	0.003	898.8	CsI, ThF_4, LIQ2, LIQ1
0.926	0.537	698.3	CsF, Cs_3ThF_7, CsI, LIQ1
0.053	0.502	682.6	CsI, Cs_2ThI_6, ThF_4, LIQ1
0.017	0.510	532.7	ThI_4, Cs_2ThI_6, ThF_4, LIQ1

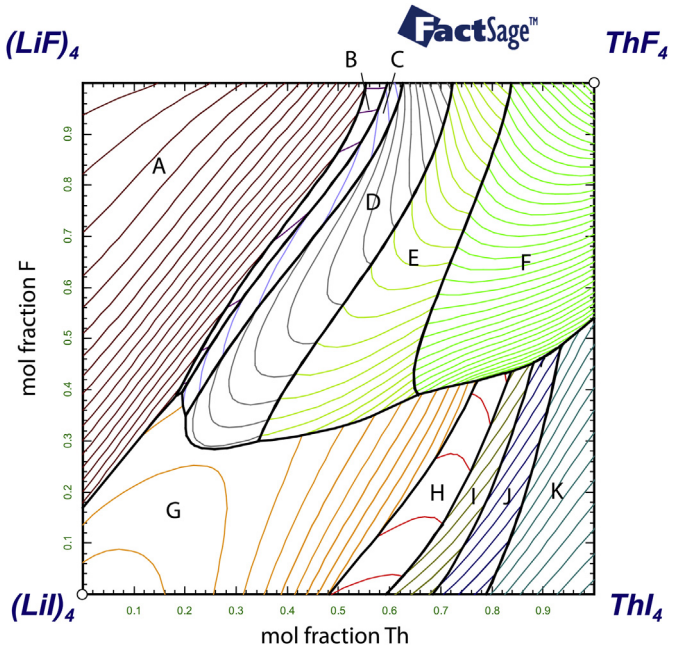

Fig. 14. The calculated liquidus projection of the Li,Th//F,I system. Prymary crystallization fields: (A) LiF (B) Li_3ThF_7; (C) $LiThF_5$ (D)$LiTh_2F_9$ (E) $LiTh_4F_{17}$ (F) ThF_4 (G) LiI (H) Li_3ThI_7 (I) $LiTh_2I_9$ (J) $LiTh_4I_{17}$ (K) ThI_4.

calculated solubility limit is exactly 1 mol%. Above this concentration a liquid-liquid miscibility gap is observed, which has a considerable effect on the fuel behaviour. In fact, the compositions of the two immiscible liquids (LIQ1 and LIQ2) are very different, one being almost a mixture of iodides and the other being almost a mixture of fluorides. Since the iodides are mainly represented by pure CsI which is rather volatile, the total vapor pressure of the fuel mixture increase dramatically (see Table 10). The same behaviour is observed for mixture containing both CsI and CsF in which the fission yield ratio (Cs:I = 10:1) is kept constant.

In conclusion, the behaviour of cesium and iodine in the fuel mixture will critically depend on the concentration. Cesium bonded to fluorine is well retained in the fuel mixture while iodine in the form of CsI has a limited solubility. When its concentration exceed about 1 mol %, CsI will precipitate and/or form a second immiscible liquid phase depending on the local temperature. This fraction of CsI is then likely to vaporize from the liquid solution.

6. Conclusions

A thermodynamic model for the Li,Th,Cs//F,I system has been developed in this work to study the behaviour of cesium and iodine in MSR fuel. The phase diagrams of nine common ion binary systems and two ternary systems have been calculated and optimized model parameters are provided. Selected compositions of the reciprocal ternary systems were measured, with particular emphasis on the LiF-CsI and ThF_4-CsI joins, and used for the assessment of the reciprocal phase diagrams. A strong short range order was observed for two of the liquid solutions, in which the first nearest neighbour pairs Cs-I and Li-F (resp. Cs-I and Th-F) predominates. The measured equilibria for the ternary LiF-CsF-ThF_4 and LiF-CsF-CsI compositions were not used to tune the thermodynamic model but agree well, with a maximum discrepancy of 13 K. Therefore, the results validate the predictive ability of the thermodynamic assessment.

Using the developed thermodynamic database, the influence of CsI and CsF, which represent the likely most stable chemical forms of cesium and iodine in the MSR fuel, was evaluated. The calculations performed in this work have shown a very different behaviour for cesium and iodine depending on their chemical form. The influence of CsF on the liquidus temperature and on the vapor pressure of the fuel mixture is negligible and cesium remains dissolved in the fluoride matrix. On the contrary, the solubility limit of CsI in the LiF-ThF_4 eutectic mixture is very small and an increase in the CsI concentration results in an increase in the fuel mixture vapor pressure. Based on these observations, CsI must be regarded as a volatile component in MSR above certain concentration and will probably be stripped to some extent to the offgas removal

Table 9
Invariant equilibria found in the Li,Th//F,I reciprocal system.

X_{Cs}	X_F	T/K	Phases in equilibrium
0.343	0.300	690.4	LiI, $LiTh_4F_{17}$, $LiTh_2F_9$, LIQ1
0.201	0.350	680.7	LiI, $LiThF_5$, $LiTh_2F_9$, LIQ1
0.194	0.395	667.5	LiI, $LiThF_5$, Li_3ThF_7, LIQ1
0.184	0.390	666.6	LiI, LiF, Li_3ThF_7, LIQ1
0.656	0.391	580.9	LiI, $LiTh_4F_{17}$, ThF_4, LIQ1
0.935	0.486	495.1	ThI_4, $LiTh_4I_{17}$, ThF_4, LIQ1
0.881	0.452	455.4	ThF_4, $LiTh_2I_9$, $LiTh_4I_{17}$, LIQ1
0.772	0.418	443.5	LiI, ThF_4, Li_3ThI_7, LIQ1

Table 10
Influence of CsI and CsF composition on the most important thermodynamic properties of the MSR fuel mixture.

Composition	Liquidus temperature	Vapour pressure 900 K	Dominant vapour species
LiF-ThF_4 (76.2–23.8)	832 K	$2.44 \cdot 10^{-3}$ Pa	LiF(g)
LiF-ThF_4-CsF (75.4-23.6-1.0)	833 K	$2.85 \cdot 10^{-3}$ Pa	LiF(g)
LiF-ThF_4-CsF (72.4-22.6-5.0)	844 K	$4.79 \cdot 10^{-3}$ Pa	CsF(g)
LiF-ThF_4-CsF (68.6-21.4-10.0)	864 K	$8.33 \cdot 10^{-3}$ Pa	CsF(g)
LiF-ThF_4-CsI (75.4-23.6-1.0)	884 K	$2.57 \cdot 10^{1}$ Pa	CsI(g)
LiF-ThF_4-CsI (72.4-22.6-5.0)	890 K	$2.64 \cdot 10^{1}$ Pa	CsI(g)
LiF-ThF_4-CsF-CsI (75.4-23.5-1.0-0.1)	898 K	$2.75 \cdot 10^{1}$ Pa	CsI(g)

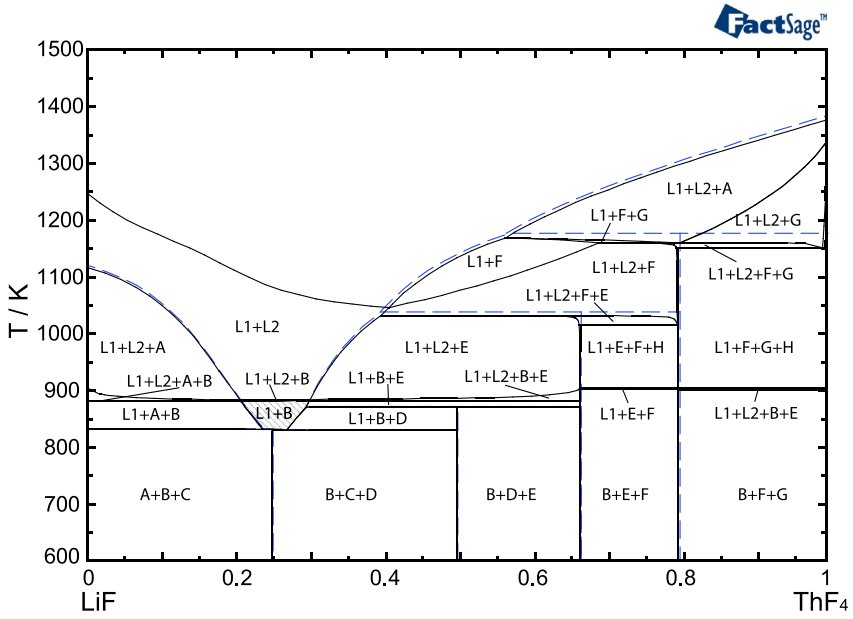

Fig. 15. The calculated pseudo binary LiF-ThF_4 with fixed concentration of CsI of 1 mol%. Indicated phases: (A) LiF (B) CsI (C) Li_3ThF_7 (D) $LiThF_5$ (E) $LiTh_2F_9$ (F) $LiTh_4F_{17}$ (G) ThF_4 (H) $CsTh_6F_{25}$. Dotted blue line: LiF-ThF_4 binary phase diagram. (For interpretation of the references to colour in this figure legend, the reader is referred to the Web version of this article.)

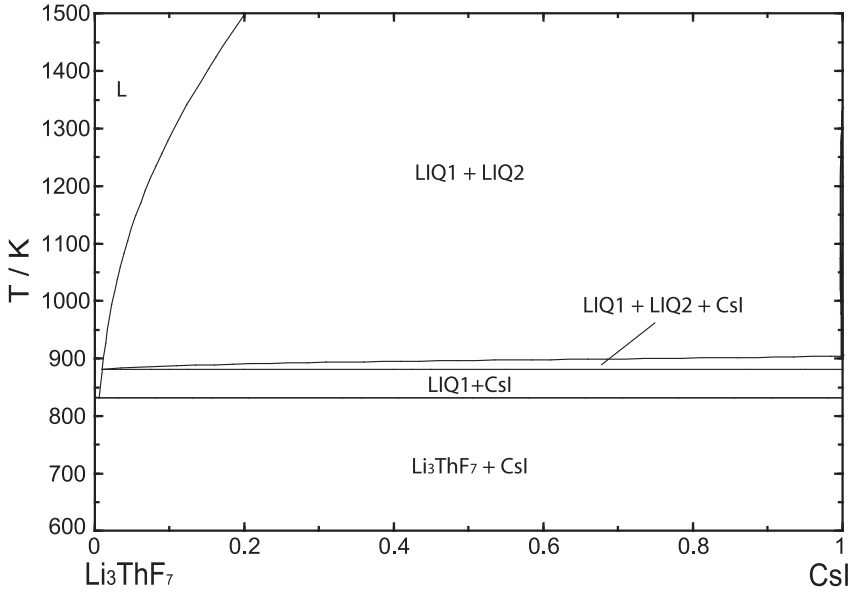

Fig. 16. The calculated pseudo binary CsI-Li_3ThF_7.

system of the reactor.

Acknowledgments

The research forms part of the Dutch programme on Molten Salt Reactor Technology, funded by the Ministry of Economic Affairs. The authors would like to thank E. Merle-Lucotte of the research group of CNRS Grenoble for the fruitful discussion.

References

[1] L. Mathieu, D. Heuer, E. Merle-Lucotte, R. Brissot, C.L. Brun, E. Liatard, J.M. Loiseaux, O. Méplan, A. Nuttin, D. Lecarpentier, Nucl. Sci. Eng. 161 (2009) 78–89.
[2] J. Serp, M. Allibert, O. Beneš, S. Delpech, O. Feynberg, V. Ghetta, D. Heuer, V. Ignatiev, J.L. Kloosterman, L. Luzzi, E. Merle-Lucotte, J. Uhlíř, R. Yoshioka, D. Zhimin, Prog. Nucl. Energ 77 (2014) 308–319.
[3] E. Capelli, O. Beneš, R.J.M. Konings, J. Nucl. Mater. 462 (2015) 43–53.
[4] E. Capelli, O. Beneš, R.J.M. Konings, J. Nucl. Mater. 449 (2014) 111–121.
[5] J. Phys. Chem. Ref. Data, Monograph, in: M.W. Chase Jr. (Ed.), NIST-JANAF Thermochemical Tables Fourth Edition, vol. 9, 1998.
[6] F.Z. Roki, M.N. Ohnet, S. Fillet, C. Chatillon, I. Nuta, J. Chem. Thermodyn. 70 (2014) 46–72.
[7] M.H. Rand, J. Fuger, I. Grenthe, V. Neck, D. Rai, Chemical Thermodynamics of Thorium, OECD Nuclear Energy Agency, Paris, 2008.
[8] O. Beneš, R.J.M. Konings, S. Wurzer, M. Sierig, A. Dockendorf, Thermochim. Acta 509 (2010) 62–66.
[9] O. Beneš, D. Sedmidubský, M. Beilmann, O.S. Valu, E. Capelli, M. Salanne, S. Nichenko, R.J.M. Konings, J. Chem. Thermodyn. 57 (2013) 92–100.
[10] N. Vozárová, A.L. Smith, J.Y. Colle, P.E. Raison, D. Bouxière, R.J.M. Konings, O. Beneš, J. Chem. Thermodyn. 114 (2017) 71–82.
[11] R.J.M. Konings, L.R. Morss, J. Fuger, The Chemistry of the Actinide and Transactinide Elements, vol. 4, Springer, Dordrecht, The Netherlands, 2006 chap. 19.
[12] V.P. Glushko, L.V. Gurvich, G.A. Bergman, I.V. Veyts, V.A. Medvedev, G.A. Khachkuruzov, V.S. Yungman, Termodinamicheskie Svoistva Individual'nykh Veshchestv. Tom IV, Nauka, Moskva .
[13] HSC Chemistry(R) 6.0, Outokumpu, 2002.
[14] P. Chartrand, A.D. Pelton, Metall. Trans. 32A (2001) 1410–1417.
[15] E. Capelli, O. Beneš, M. Beilmann, R.J.M. Konings, J. Chem. Thermodyn. 58 (2013) 110–116.
[16] G.A. Bukhalova, D.V. Sementsova, Russ. J. Inorg. Chem. 10 (1965) 1024–1026.
[17] R.E. Thoma, Advances in Molten Salt Chemistry, vol. 3, Plenum Press, 1975, p. 275 chap. 6.
[18] J.L. Holm, O.J. Kleppa, J. Chem. Phys. 49 (1968) 2425–2430.
[19] J. Sangster, A.D. Pelton, J. Phys. Chem. Ref. Data 16 (1987) 509–561.
[20] O. Beneš, R.J.M. Konings, Computer Coupling of Phase Diagrams and Thermochemistry, vol 32, 2008, pp. 121–128.
[21] G.A. Bukhalova, G.A. Shegurova, T.M. Khliyan, E.S. Yagub'yan, Russ. J. Inorg. Chem. 18 (1973) 583.
[22] E.C. Johnson, E.J. Hathaway, J. Electrochem. Soc. 118 (1971) 631–634.
[23] M.E. Melnichak, O.J. Kleppa, J. Chem. Phys. 52 (1970) 1790–1794.
[24] W. Brendel, T. Samartzis, C. Brendel, B. Krebs, Thermochim. Acta 83 (1985) 167–172.
[25] G.J. Janz, C.B. Allen, J.R. Downey, R.P.T. Tomkins, NSRDS-NBS-61 Part I, Technical Report, National Bureau of Standards, 1978. p.41.
[26] N. Vozárová, Behaviour of Fission Products in the Molten Salt Reactor Fuel, Master's thesis, ETH Zurich, 2016.
[27] E.M. Dvoryanova, I.M. Kondratyuk, I.K. Garkushin, Russ. J. Inorg. Chem. 55 (2010) 1136–1141.
[28] E.M. Dvoryanova, Physico-chemical Interaction in Systems Involving Fluorides and Iodides of Alkali Metals (Russian), Ph.D. thesis, Samara State Technical University, 2008.
[29] C. Margheritis, G. Flor, C. Sinistri, Z. Naturforsch, 28a (1973) 1329–1334.
[30] M. Brovchenko, Études préliminaires de sûreté du réacteur à sels fondus MSFR (French), Ph.D. thesis, Université de Grenoble, 2013.
[31] G. Duran-Klie, Étude du comportment de l'uranium et de l'iode dans le mélange de fluorures fondus LiF-ThF à 650 C (French), Ph.D. thesis, Université Paris-Saclay, 2017.
[32] A. Laureau, D. Heuer, E. Merle-Lucotte, P.R. Rubiolo, M. Allibert, M. Aufiero, Nucl. Eng. Des. 316 (2017) 112–124.